Competing spin-valley entangled and broken symmetry states in the $N = 1$ Landau level of graphene

Nikolaos Stefanidis [1,*] and Inti Sodemann Villadiego [2,1,†]
[1] Max-Planck-Institut für Physik komplexer Systeme, Dresden 01187, Germany
[2] Institut für Theoretische Physik, Universität Leipzig, D-04103, Leipzig, Germany

(Received 24 October 2022; revised 23 December 2022; accepted 3 January 2023; published 23 January 2023)

The nature of states in the quantum Hall regime of graphene in higher Landau levels remains poorly understood partly because of the lack of a model that captures its valley-dependent symmetry breaking interactions. In this paper we develop systematically such a model, which interestingly, and in contrast to the $N = 0$ Landau level, features not only pure δ function interactions, but also some of its derivatives. We show that this model can lead to qualitatively new ground states relative to the $N = 0$ Landau level, such as ground states with entangled spin and valley degrees of freedom that compete with simpler broken symmetry states. Moreover, at half-filling we have found a new phase that is absent in the $N = 0$ Landau level which combines characteristics of a valence-bond solid and an antiferromagnet. We discuss the estimation of parameters of this model based on recent compressibility experiments.

DOI: 10.1103/PhysRevB.107.045132

I. INTRODUCTION

The quantum Hall regime in graphene realizes a rich landscape of broken symmetry and topological states, stemming, in part, from the near fourfold degeneracy of its Landau levels (LLs) associated with its valley and spin degrees of freedom [1]. Most studies to date have focused in the $N = 0$ LL with transport and magnon transmission experiments favoring an antiferromagnetic (AF) state at neutrality [2–6], whereas scanning tunnel microscope (STM) experiments reporting evidence for Kekulé-type valence-bond solids and charge density-wave states (CDW) [7–9].

However, the nature of states realized in the $N = 1$ LL and higher LLs of graphene remains a widely open problem. Understanding these higher Landau levels is important because they could harbor fundamentally new quantum states of matter with no analogs in other material platforms. For example, Ref. [10] reported evidence for even denominator states in the $N = 3$ LL of monolayer graphene. This is a highly unusual observation because in traditional two-dimensional electron systems there are no fractional quantum Hall (FQH) states at such high Landau levels but rather broken symmetry states, such as stripes tend to appear [11]. The fact that non-Abelian FQH states tend to appear in higher Landau levels, makes the case for truly exotic states [10] a provocative one.

But one of the main obstacles that hinders developing a precise understanding of these intriguing higher LLs of graphene is the lack of a model that systematically captures their valley-dependent symmetry-breaking interactions. Therefore, one of the main purposes of our paper is precisely to derive such a model. We will show that, interestingly and in contrast to the $N = 0$ LL [12], the $N = 1$ LL model contains interactions that are not pure δ functions [13].

Our second important goal will be to determine the ground states of this model at various partial integer fillings. We will show that these states can be qualitatively distinct from those realized in the $N = 0$ LL. For example, at quarter-filling (to be denoted by $\tilde{\nu} = 1$). We will show that the model can have ground states that are spin-valley entangled. Moreover, when two components are filled (to be denoted by $\tilde{\nu} = 2$), we will show that a new type of Kekulé-antiferromagnetic state appears which is absent in the $N = 0$ LL. We will see that based on the parameters estimated in Ref. [13], graphene is expected to be in a delicate competition between an AF and a CDW state. However, as we will discuss, these parameters are possibly missing some important terms.

II. MODEL AND SYMMETRIES

Although the long-range part of the Coulomb interaction is typically the dominant term in the Hamiltonian, it possesses a large degree of symmetry that leaves the quantum Hall ground states undetermined. Therefore, it is crucial to account for the corrections that reflect the lower symmetry of the underlying graphene lattice to select the ground states [1,12,14–18]. A convenient model to capture these symmetry-breaking interactions in the $N = 0$ LL was introduced by Kharitonov in Ref. [12]. This model can be viewed as a projection into the $N = 0$ LL of a more general model introduced by Kharitonov [12] and Aleiner *et al.* [19] that includes all possible δ-function interactions allowed by symmetries. There is no study to this date that has constructed an analogous model in the $N = 1$ LL that includes all possible short-distance

*nikos@pks.mpg.de
†sodemann@itp.uni-leipzig.de

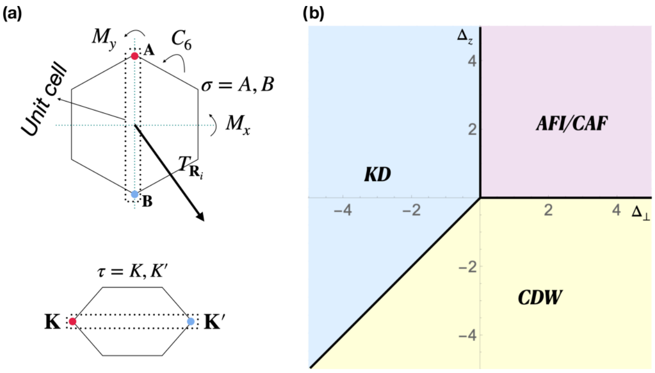

FIG. 1. (a) Graphene unit cell and its lattice symmetries (top) and its reciprocal unit cell (bottom). (b) Phase diagram at $\tilde{\nu} = 1$. It contains four phases: CDW, KD, and the two entangled phases, the AFI and the CAF.

interactions allowed by symmetry, although a related model containing some of these terms was introduced in Ref. [13].

We begin by reviewing the continuum model of short-range symmetry-breaking interactions of Aleiner *et al.* [19] in the absence of a magnetic field. This is described by the following Hamiltonian:

$$\mathcal{H} = \mathcal{H}_D + \mathcal{H}_C + \mathcal{H}_A, \tag{1}$$

with

$$\mathcal{H}_D = v_F \sum_i \left(\tau_z^i p_x^i \sigma_x^i + p_y^i \sigma_y^i\right) \tag{2}$$

being the linearized single-particle Hamiltonian around the Dirac points,

$$\mathcal{H}_C = \sum_{i<j} \frac{e^2}{\epsilon |\mathbf{r}_i - \mathbf{r}_j|},$$

the Coulomb interaction, and

$$\mathcal{H}_A = \sum_{i<j} \left\{ \sum_{\alpha,\beta} V_{\alpha\beta} T^i_{\alpha\beta} T^j_{\alpha\beta} \right\} \delta(\mathbf{r}_i - \mathbf{r}_j), \tag{3}$$

the sublattice-valley-dependent interactions. We have defined $T^{i(j)}_{\alpha\beta} = \tau^{i(j)}_\alpha \otimes \sigma^{i(j)}_\beta \otimes s^{i(j)}_0$, and $\tau^{i(j)}_\alpha$, $\sigma^{i(j)}_\beta$, $s^{i(j)}_0$ α, and $\beta = 0, x, y, z$ to be the Pauli matrices acting on valley, sublattice, and spin, respectively.

By denoting the valley (sublattice) states as $|\tau\rangle(|\sigma\rangle)$ with $\tau(\sigma) = \pm 1$ corresponding to the K, K' (A, B) valleys (sublattices), then the action of lattice symmetry on these states is given by

$$\begin{aligned}
C_6|\tau,\sigma\rangle &= Z^{-\tau\sigma}|-\tau,-\sigma\rangle,\\
M_x|\tau,\sigma\rangle &= |\tau,-\sigma\rangle,\\
M_y|\tau,\sigma\rangle &= |-\tau,\sigma\rangle,\\
T_{R_{1,2}}|\tau,\sigma\rangle &= Z^{\pm\tau}|\tau,\sigma\rangle,
\end{aligned} \tag{4}$$

with $Z = e^{i(2\pi/3)}$. C_6 is the rotation by $\pi/3$, M_x, and M_y the two mirrors and T_{R_i} the translations by the two basis vectors of graphene [see Fig. 1(a) for the illustration of these symmetries]. These symmetries reduce the couplings of Eq. (3) to nine independent couplings satisfying the following relations [19]:

$$\begin{aligned}
F_{\perp z} &\equiv V_{xx} = V_{yx},\\
F_{z\perp} &\equiv V_{0x} = V_{zy},\\
F_{\perp\perp} &\equiv V_{xz} = V_{y0} = V_{yz} = V_{x0},\\
F_{0\perp} &\equiv V_{zx} = V_{0y},\\
F_{\perp 0} &\equiv V_{yy} = V_{xy},\\
F_{zz} &\equiv V_{0z},\\
F_{z0} &\equiv V_{z0},\\
F_{0z} &\equiv V_{zz}.
\end{aligned} \tag{5}$$

III. PROJECTED MODEL IN THE $N = 1$ LANDAU LEVEL

By projecting $\mathcal{H}_A$ from Eq. (1) with the constraints in Eq. (5), one obtains the following Hamiltonian of symmetry-breaking interactions in the Nth LL:

$$\mathcal{H}_A^N = \sum_{i<j} \left\{ V_z^N(r_{ij})\tau_z^i\tau_z^j + V_\perp^N(r_{ij})\tau_\perp^i\tau_\perp^j \right\}, \tag{6}$$

with $\tau_\perp^i\tau_\perp^j = \tau_x^i\tau_x^j + \tau_y^i\tau_y^j$ (see section S-II of [20] for further details). As we see, there is an effective $U(1)$ valley conservation arising from the underlying lattice symmetries. Specifically, for the $N = 1$ LL we have

$$V_{z,\perp}(r_{ij}) = \sum_{n=0}^{2} g_n^{z,\perp} \nabla^{2n} \delta(r_{ij}). \tag{7}$$

Here $g_n^{z,\perp}$ are independent constants that parametrize the projected interactions that are linear combinations of those in Eq. (5) [20]. Therefore, we have a model with six independent parameters characterizing the interactions in the $N = 1$ LL, in contrast to the more restricted model of Ref. [13] with only two parameters. The model of Ref. [13] is a special case of our Eq. (7) in which $g^z_{0,1} = g^\perp_{0,2} = 0$. Note, in particular, that in our model the $n = 0$ terms in Eq. (7) are pure δ-function interactions, which are absent in Ref. [13] (see section S-IV of [20] for further details).

On the other hand, if we project $\mathcal{H}_A$ onto the $N = 0$ LL we obtain the model from Ref. [12] for which the interactions would include only pure δ functions (see section S-II of [20] for further details),

$$V_{z,\perp}(r_{ij}) = g_{z,\perp}\delta(r_{ij}). \tag{8}$$

Therefore, the main difference between the model of Eq. (7) for the $N = 1$ LL and the model of Ref. [12] for the $N = 0$ LL is the existence of interactions which are not pure δ functions.[1] As we will show, this leads to several important differences in the physics of these two Landau levels.

[1] We are neglecting Landau-level mixing effects that can generate interactions with a longer range than δ functions as explained in Ref. [21].

IV. MEAN-FIELD GROUND STATES

We will now derive the Hartree-Fock (HF) functional for the Hamiltonian of Eqs. (6) and (7) and obtain the phase diagram in the integer fillings of the $N = 1$ LL, $\tilde{\nu} = 1$ ($\tilde{\nu} = 2$) when one (two) out of the four valley-spin degenerate LLs are filled.[2] We consider the competition of translational invariant integer quantum Hall ferromagnets that can be described by a particle-hole condensate order parameter of the form $\langle c^\dagger_{X_1\tau_1 s_1} c_{X_2\tau_2 s_2}\rangle = P^{s_1 s_2}_{\tau_1\tau_2}\delta_{X_1,X_2}$ with X_i labeling intra-LL guiding center coordinates. Here $c^\dagger_{X\tau s}$ denotes the electron creation operator with valley τ and spin s, and P is the projector in spin-valley space into either a one-dimensional subspace (for $\tilde{\nu} = 1$) or a two-dimensional subspace (for $\tilde{\nu} = 2$). The general form of the Hartree-Fock functional is then ($\mathcal{E}_{\mathrm{HF}}[P] \equiv \frac{2A}{N_\phi^2} E_{\mathrm{HF}}[P]$),

$$\mathcal{E}_{\mathrm{HF}}[P] = \sum_{i=x,y,z} \left[u_i^H (\mathrm{Tr}\{T_i P\})^2 - u_i^X \mathrm{Tr}\{(T_i P)^2\}\right], \tag{9}$$

with $u_\perp^{H,X} = u_x^{H,X} = u_y^{H,X}$. Therefore, the possible ground states depend only on four effective Hartree and exchange constants, u_z^H, u_z^X, $u_\perp^H$, $u_\perp^X$, which are linear combinations of the constants $g_n^{z,\perp}$ that appear in Eq. (7). Moreover, whereas in the $N = 0$ LL the Hartree and the exchange constants are forced to be equal, $u^H_{z,\perp} = u^X_{z,\perp}$ [12], in the $N = 1$ LL they are independent due to the appearance of non-δ interactions (see section S-III of [20] for further details). Similar functionals have been proposed, however, phenomenologically for the $N = 0$ LL to capture the physics beyond the δ functions in Refs. [21,22].

We will consider general spin-valley entangled variational states [21–24]. The following two orthonormal spinors can be used to uniquely parametrize the state characterized by P in Eq. (9),

$$|F\rangle_1 = \cos\frac{a_1}{2}|\boldsymbol{\eta}\rangle|\mathbf{s}\rangle + e^{i\beta_1}\sin\frac{a_1}{2}|-\boldsymbol{\eta}\rangle|-\mathbf{s}\rangle,$$
$$|F\rangle_2 = \cos\frac{a_2}{2}|\boldsymbol{\eta}\rangle|-\mathbf{s}\rangle + e^{i\beta_2}\sin\frac{a_2}{2}|-\boldsymbol{\eta}\rangle|\mathbf{s}\rangle. \tag{10}$$

Here $|\boldsymbol{\eta}\rangle$ and $|\mathbf{s}\rangle$ are states parametrized by unit vectors $\boldsymbol{\eta}$ and $\mathbf{s}$ in the spin and valley Bloch spheres, respectively, and $a_{1,2}$ and $\beta_{1,2}$ are real constants. Note that, in general, these states might not be separable into a tensor product of spin and valley components and, therefore, can account for spin-valley entanglement [22]. For $\tilde{\nu} = 1$, we take $P = |F_1\rangle\langle F_1|$, and for $\tilde{\nu} = 2$, $P = |F_1\rangle\langle F_1| + |F_2\rangle\langle F_2|$.

V. GROUND STATES FOR $\tilde{\nu} = 1$

As discussed in Ref. [22], the energy functional in this case reduces to

$$\mathcal{E}_{\mathrm{HF}}^{\tilde{\nu}=1} = \cos^2 a_1 \left\{\Delta_z \eta_z^2 + \Delta_\perp \eta_\perp^2\right\}, \tag{11}$$

with $\Delta_z = u_z^H - u_z^X$, $\Delta_\perp = u_\perp^H - u_\perp^X$, and $\eta_\perp^2 = \eta_x^2 + \eta_y^2$ (see section S-V-A) of [20] for further details). The resulting phase diagram is shown in Fig. 1(b) and contains four phases. These are a CDW with $\boldsymbol{\eta} = \hat{z}$, $\boldsymbol{s} = \hat{z}$, and $a_1 = 0$, and a Kekulé distortion (KD) state with $\boldsymbol{\eta} = \boldsymbol{\eta}_\perp$, $\boldsymbol{s} = \hat{z}$, and $a_1 = 0$. Interestingly, we see that also spin-valley entangled phases with $a_1 = \pi/2$, appear when $\Delta_z > 0$ and $\Delta_\perp > 0$. These entangled phases are degenerate in the absence of Zeeman fields, but in their presence, they split antiferrimagnetic phase (AFI) with $\boldsymbol{\eta} = \hat{z}$, $\boldsymbol{s} = \hat{z}$, and $a_1 = \frac{\pi}{2}$ and the canted antiferromagnet (CAF) with $\boldsymbol{\eta} = \boldsymbol{\eta}_\perp$, $\boldsymbol{s} = \hat{z}$, and $a_1 = \frac{\pi}{2}$ as discussed in Ref. [22].

Note that in the $N = 0$ LL, $\Delta_z = \Delta_\perp = 0$, and, therefore, all of the above states would be degenerate and with a vanishing HF energy.

TABLE I. Competing states at $\tilde{\nu} = 2$ and their wave functions.

States appearing at $\tilde{\nu} = 2$	
States	Wave functions $\{\lvert F\rangle_1, \lvert F\rangle_2\}$
CDW	$\{\lvert\hat{z}\rangle\ \lvert\mathbf{s}\rangle,\ \lvert\hat{z}\rangle\ \lvert-\mathbf{s}\rangle\}$
KD	$\{\lvert\boldsymbol{\eta}_\perp\rangle\ \lvert\mathbf{s}\rangle,\ \lvert\boldsymbol{\eta}_\perp\rangle\ \lvert-\mathbf{s}\rangle\}$
Ferromagnet	$\{\lvert\hat{z}\rangle\ \lvert\mathbf{s}\rangle,\ \lvert-\hat{z}\rangle\ \lvert\mathbf{s}\rangle\}$
AF	$\{\lvert\hat{z}\rangle\lvert\mathbf{s}\rangle,\ \lvert-\hat{z}\rangle\lvert-\mathbf{s}\rangle\}$
Kekulé antiferromagnet (KD-AF)	$\{\lvert\boldsymbol{\eta}_\perp\rangle\lvert\mathbf{s}\rangle,\ \lvert-\boldsymbol{\eta}_\perp\rangle\lvert-\mathbf{s}\rangle\}$

VI. GROUND STATES FOR $\tilde{\nu} = 2$

The HF functional for $\nu = 2$ is more difficult to minimize analytically. To make progress, we first consider the subset of states from Eq. (10) without spin-valley entanglement. These can be classified into the valley active states [25],

$$|F\rangle_1 = |\boldsymbol{\eta}_1\rangle|\mathbf{s}\rangle, \quad |F\rangle_2 = |\boldsymbol{\eta}_2\rangle|-\mathbf{s}\rangle, \tag{12}$$

in which the valley degree of freedom varies, and the spin active states,

$$|F\rangle_1 = |\boldsymbol{\eta}\rangle|\mathbf{s}_1\rangle, \quad |F\rangle_2 = |-\boldsymbol{\eta}\rangle|\mathbf{s}_2\rangle, \tag{13}$$

in which the spin degree of freedom varies. We first minimize the energy functional within this subspace and then perform a quadratic expansion of all possible deviations of parameters that account for spin-valley entangled states (see sections S-V-B), VI, VII of [20] for further details. For simplicity we will also neglect the Zeeman term that is typically weak compared to the interaction terms [2,26,27]. In contrast to $\tilde{\nu} = 1$ for $\tilde{\nu} = 2$ we find that whenever a spin-valley disentangled state is energetically favorable it is also an exact local minima of the energy with respect to all possible quadratic deviations that include spin-valley entanglement. This indicates that these spin-valley disentangled states are also possibly exact global minima of the energy.

Following this procedure, we find a total of five possible ground states for $\tilde{\nu} = 2$ that are realized as a function of the four Hartree and exchange parameters u_z^H, u_z^X, $u_\perp^H$, and $u_\perp^X$. These possible five states are listed in Table I (see section S-V-B) of [20] for further details). To visualize the energetic competition among these five phases, we have chosen to draw two-dimensional phase diagrams as functions of the two Hartree parameters $\tilde{u}^H_{z,\perp} = u^H_{z,\perp}/|\Delta_z - \Delta_\perp|$ for fixed values of $\Delta_z = u_z^H - u_z^X$ and $\Delta_\perp = u_\perp^H - u_\perp^X$. We find that there are a

[2]The partial filling of $\tilde{\nu} = 3$ ($\tilde{\nu} = 2$) is equivalent to $\tilde{\nu} = 1$ ($\tilde{\nu} = 4$) by a particle-hole conjugation.

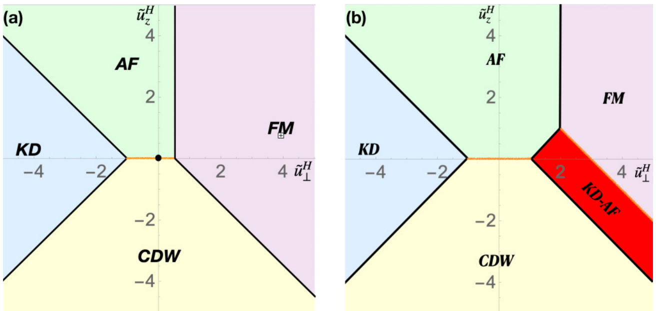

FIG. 2. (a) Phase diagram at $\tilde{\nu} = 2$ when $\Delta_z < 0$, $\Delta_\perp > 0$, and|; $\Delta_z < \Delta_\perp$ for $\Delta_z/\Delta_\perp = -1$. According to the estimates of Ref. [13] (see section S-II of [20] for further details), graphene is located at the dot at the origin and, therefore, at the boundary between the CDW and AF phases. (b) Phase diagram at $\tilde{\nu} = 2$ when Δ_z, $\Delta_\perp > 0$, $\Delta_z < \Delta_\perp$ for $\Delta_z/\Delta_\perp = 1/2$. This contains a new phase, the KD-AF, which does not appear in the $N = 0$ LL. The thick black boundaries represent special first-order transitions (phases become unstable coincidentally with their energy crossing) whereas the orange ones indicate ordinary first-order transitions (energies cross but phases remain metastable).

total of seven different kinds of phase diagrams depending on the values and signs of $\Delta_{z,\perp}$. Two of these representative phase diagrams are depicted in Fig. 2, and the remainder are presented in (see section S-V-B) of Ref. [20] for further details).

Interestingly, according to the model and the estimates of Ref. [13], $u_z^H = u_\perp^H = 0$, $u_z^X > 0$, and $u_\perp^X < 0$ (see section S-IV of [20] for further details). This means that graphene in the $N = 1$ LL would have a phase diagram, such as the one in Fig. 2(a), and it would be located exactly at the origin of this phase diagram, which we indicate by a black dot in Fig. 2(a). Therefore, we see that the model and the parameter estimates of Ref. [13] place graphene right at the boundary between the CDW and the AF states. We note that even at this boundary, these phases remain stable against spin-valley entangled rotations (see section S-VII of [20] for further details).

One of the interesting qualitative differences that we have found in the $N = 1$ LL is the existence of a new phase that features a combination of Kekulé state and antiferromagnet, that we term the KD-AF. In this phase one set of electrons has an XY vector in the valley sphere with spin up whereas the others occupy the opposite valley vector with spin down as described in Table I. This phase occupies the red region in Fig. 2(b).

In Figs. 2(a) and 2(b) the phase transitions represented by black thick lines are a special type of first-order transitions, in the sense that at these lines the energy of two states is the same, and the quadratic expansion around them indicates an instability (or, in other words, the states do not remain metastable upon crossing this line). This makes these boundaries interesting as they are expected to be highly sensitive to perturbations which could lead to new phases or phase coexistence as discussed in Ref. [21], and they could harbor larger symmetries, as in the $SO(5)$ symmetry in the AF-Kekulé transition found in the $N = 0$ LL [28]. The phase transitions represented by orange lines indicate ordinary first-order transitions, namely, at these lines there is an energy crossing between two states but both of these states remain metastable in the immediate vicinity of these lines.

VII. DISCUSSION

We have constructed a general model consistent with the lattice symmetries of graphene that describes the short-range corrections to the Coulomb interaction in its higher LLs. We have applied, in particular, this model to determine the spontaneous symmetry-broken ground states at integer fillings of the $N = 1$ LL. We have found several important qualitative differences with respect to the $N = 0$ LL. First, we showed that when a single component of the $N = 1$ LL is filled ($\tilde{\nu} = 1$), our model can lift the degeneracy to select the ground states, in contrast to the $N = 0$ LL where states remain undetermined. Moreover, interestingly, among the possible competing states at $\tilde{\nu} = 1$, we find that spin-valley entangled phases can appear. On the other hand, when two components are filled ($\tilde{\nu} = 2$), we have found a qualitatively new state that is absent in the $N = 0$ LL, which features a combination of Kekulé and antiferromagnet character and that we have termed the Kekulé-antiferromagnet state. We caution that phases in the $N = 1$ LL which nominally have the same spin-valley vector as their counterparts in the $N = 0$ LL, might still experimentally look quite different, for example, in STM measurements because of the different orbital character of the $N = 1$ LL vs $N = 0$ LL orbitals.[3]

We have shown that the related model for the $N = 1$ LL that appeared in Ref. [13] is missing terms that are allowed by symmetry and is a special case of our model (6). In particular, Ref. [13] is missing the intersublattice scattering interactions that appear in Eq. (3). By taking the parameters from Ref. [13], we find that graphene will be near the phase boundary separating the CDW and AF states. However, this prediction should be taken carefully because of the aforementioned absence of A-B scattering processes in the model of Ref. [13]. These processes are known to be crucial in the $N = 0$ LL, because they give rise to "$g_\perp$" interaction in Eq. (8) that ultimately is needed to stabilize the AF or Kekulé states that are reported in experiments [7–9,13,29]. We see no reason why these intersublattice scattering terms would be negligible in the higher Landau levels. We hope our paper stimulates future experiments to better narrow down the states and parameters realized in the $N = 1$ and higher LLs of graphene.

[3]Despite these differences, phases in the $N = 1$ LL vs $N = 0$ LL with the same spin-valley vectors would have the same pattern of spin and lattice point-group symmetry breaking.

[1] M. O. Goerbig, Electronic properties of graphene in a strong magnetic field, Rev. Mod. Phys. **83**, 1193 (2011).

[2] A. Young, J. Sanchez-Yamagishi, B. Hunt, S. Choi, K. Watanabe, T. Taniguchi, R. Ashoori, and P. Jarillo-Herrero, Tunable symmetry breaking and helical edge transport in a

graphene quantum spin hall state, Nature (London) **505**, 528 (2014).

[3] D. S. Wei, T. Van Der Sar, S. H. Lee, K. Watanabe, T. Taniguchi, B. I. Halperin, and A. Yacoby, Electrical generation and detection of spin waves in a quantum hall ferromagnet, Science **362**, 229 (2018).

[4] P. Stepanov, S. Che, D. Shcherbakov, J. Yang, R. Chen, K. Thilahar, G. Voigt, M. W. Bockrath, D. Smirnov, K. Watanabe *et al.*, Long-distance spin transport through a graphene quantum hall antiferromagnet, Nat. Phys. **14**, 907 (2018).

[5] H. Zhou, C. Huang, N. Wei, T. Taniguchi, K. Watanabe, M. P. Zaletel, Z. Papić, A. H. MacDonald, and A. F. Young, Strong-Magnetic-Field Magnon Transport in Monolayer Graphene, Phys. Rev. X **12**, 021060 (2022).

[6] A. K. Paul, M. R. Sahu, K. Watanabe, T. Taniguchi, J. Jain, G. Murthy, and A. Das, Electrically switchable tunneling across a graphene pn junction: evidence for canted antiferromagnetic phase in $\nu = 0$ state, arXiv:2205.00710.

[7] S.-Y. Li, Y. Zhang, L.-J. Yin, and L. He, Scanning tunneling microscope study of quantum hall isospin ferromagnetic states in the zero landau level in a graphene monolayer, Phys. Rev. B **100**, 085437 (2019).

[8] X. Liu, G. Farahi, C.-L. Chiu, Z. Papic, K. Watanabe, T. Taniguchi, M. P. Zaletel, and A. Yazdani, Visualizing broken symmetry and topological defects in a quantum hall ferromagnet, Science **375**, 321 (2022).

[9] A. Coissard, D. Wander, H. Vignaud, A. G. Grushin, C. Repellin, K. Watanabe, T. Taniguchi, F. Gay, C. B. Winkelmann, H. Courtois *et al.*, Imaging tunable quantum hall broken-symmetry orders in graphene, Nature (London) **605**, 51 (2022).

[10] Y. Kim, A. C. Balram, T. Taniguchi, K. Watanabe, J. K. Jain, and J. H. Smet, Even denominator fractional quantum hall states in higher landau levels of graphene, Nat. Phys. **15**, 154 (2019).

[11] M. P. Lilly, K. B. Cooper, J. P. Eisenstein, L. N. Pfeiffer, and K. W. West, Evidence for an Anisotropic State of Two-Dimensional Electrons in High Landau Levels, Phys. Rev. Lett. **82**, 394 (1999).

[12] M. Kharitonov, Phase diagram for the $\nu = 0$ quantum hall state in monolayer graphene, Phys. Rev. B **85**, 155439 (2012).

[13] F. Yang, A. A. Zibrov, R. Bai, T. Taniguchi, K. Watanabe, M. P. Zaletel, and A. F. Young, Experimental Determination of the Energy per Particle in Partially Filled Landau Levels, Phys. Rev. Lett. **126**, 156802 (2021).

[14] K. Nomura and A. H. MacDonald, Quantum Hall Ferromagnetism in Graphene, Phys. Rev. Lett. **96**, 256602 (2006).

[15] M. O. Goerbig, R. Moessner, and B. Douçot, Electron interactions in graphene in a strong magnetic field, Phys. Rev. B **74**, 161407(R) (2006).

[16] J. Alicea and M. P. A. Fisher, Graphene integer quantum hall effect in the ferromagnetic and paramagnetic regimes, Phys. Rev. B **74**, 075422 (2006).

[17] I. F. Herbut, Theory of integer quantum hall effect in graphene, Phys. Rev. B **75**, 165411 (2007).

[18] J. Jung and A. H. MacDonald, Theory of the magnetic-field-induced insulator in neutral graphene sheets, Phys. Rev. B **80**, 235417 (2009).

[19] I. L. Aleiner, D. E. Kharzeev, and A. M. Tsvelik, Spontaneous symmetry breaking in graphene subjected to an in-plane magnetic field, Phys. Rev. B **76**, 195415 (2007).

[20] See Supplemental Material at http://link.aps.org/supplemental/10.1103/PhysRevB.107.045132 for the projected model in the Nth Landau level, the Hartree-fock theory, and its ground states and the linear stability analysis.

[21] A. Das, R. K. Kaul, and G. Murthy, Coexistence of Canted Antiferromagnetism and Bond Order in $\nu = 0$ Graphene, Phys. Rev. Lett. **128**, 106803 (2022).

[22] J. Atteia and M. O. Goerbig, SU(4) spin waves in the $\nu = \pm 1$ quantum hall ferromagnet in graphene, Phys. Rev. B **103**, 195413 (2021).

[23] Y. Lian and M. O. Goerbig, Spin-valley skyrmions in graphene at filling factor $\nu = -1$, Phys. Rev. B **95**, 245428 (2017).

[24] J. Atteia, Y. Lian, and M. O. Goerbig, Skyrmion zoo in graphene at charge neutrality in a strong magnetic field, Phys. Rev. B **103**, 035403 (2021).

[25] S. S. Hegde and I. S. Villadiego, Theory of competing charge density wave, kekulé, and antiferromagnetically ordered fractional quantum hall states in graphene aligned with boron nitride, Phys. Rev. B **105**, 195417 (2022).

[26] D. A. Abanin, B. E. Feldman, A. Yacoby, and B. I. Halperin, Fractional and integer quantum hall effects in the zeroth landau level in graphene, Phys. Rev. B **88**, 115407 (2013).

[27] I. Sodemann and A. H. MacDonald, Broken $SU(4)$ Symmetry and the Fractional Quantum Hall Effect in Graphene, Phys. Rev. Lett. **112**, 126804 (2014).

[28] F. Wu, I. Sodemann, Y. Araki, A. H. MacDonald, and T. Jolicoeur, SO(5) symmetry in the quantum hall effect in graphene, Phys. Rev. B **90**, 235432 (2014).

[29] F. Amet, A. Bestwick, J. Williams, L. Balicas, K. Watanabe, T. Taniguchi, and D. Goldhaber-Gordon, Composite fermions and broken symmetries in graphene, Nat. Commun. **6**, 5838 (2015).